periment anticipating high accuracy measurement. After 40 hours of monitoring time, the blue-shift reached an equilibrium state. The total wavelength change was ~2 nm.

In summary, we have conducted a systematical investigation of the $H_2$-diffusion impact on LPGs. The $H_2$-diffusion process in LPGs was significantly more complex and dynamic than in FBGs.

## CWF70

### Arbitrary spectral response fibre edge filters based on tilted chirped grating structures

Y. Liu, L. Zhang, I. Bennion, *Photonics Research Group, Division of Electronic Engineering & Computer Science, Aston University, Aston Triangle, Birmingham, B4 7ET, United Kingdom; E-mail: Liuy@aston.ac.uk*

Optical edge-filters are useful devices for interrogating fibre Bragg grating (FBG) sensors based on optical intensity measurement, providing advantages of low-cost, fast response and ease of use.[1] In this paper, we report a novel method for fabricating fibre edge filters with arbitrary spectral response based upon tilted-chirped-grating (TCG) structures.

Tilted uniform-period FBGs have been used to flatten the gain-band of EDFA by out-taping the light around 1530 nm-region. This out-tapping function results from the enhanced coupling between the guided light in the core and the radiation field.[2] The radiation mode out-coupling proportional to the tilt-angle generates a transmission loss peak at the short wavelength side of the Bragg resonance. In the case of a tilted broadly chirped grating, the loss peak is spectrally superimposed on the broad Bragg resonance, therefore, resulting in one broad transmission loss peak. The spectral response of this loss peak depends on the tilt-angle, chirp-rate and grating-strength. It is this dependence which provides a basis for designing and fabricating fibre edge-filters.

The TCGs were UV holographically side-written into hydrogenated B/Ge co-doped and standard fibres using the dissimilar wavefront method. The fibre was mounted on a rotation stage accommodating fibre-tilting operation. A set of chirped gratings were produced in each fibre for study of the relationship between the spectral response and tilt-angle, chirp-rate and grating-strength.

Figure 1(a) plots the transmission profiles of four TCGs with an 18 nm chirp rate for tilt angles of 0°, 6°, 8° and 10°. The 0°-tilted chirped grating gives a near-square-like transmission response and there is negligible radiation mode out-coupling at the short wavelength side. When the chirped grating is tilted, a remarkably broadened transmission loss peak with slightly asymmetric slopes is formed, giving a typical edge-filer profile. As the tilt-angle increases, the loss peak broadens while its centre shifts to the long wavelength direction. The slope-efficiency decreases as the grating strength decreases.

Figure 1(b) plots the transmission profiles of three gratings with chirp-rates of 8 nm, 12 nm and 16 nm for an 8°-tilt angle. The band-

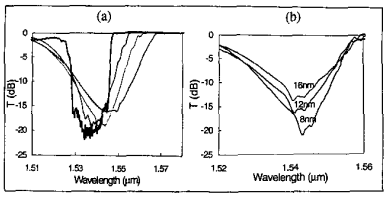


**CWF70 Fig. 1.** Spectral responses: (a) for different tilted angles; (b) for different chirp rates.

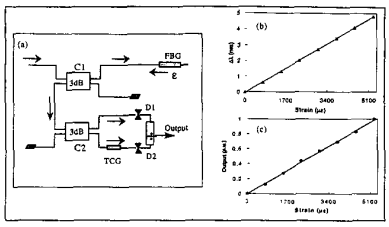


**CWF70 Fig. 2.** (a) Strain interrogation system; (b) Wavelength shift against strain from optical spectrum analyser; (c) Optical power against strain from photodiodes.

widths and the centres are very similar for three different chirp-rates indicating they are only tilt-angle dependent, but the slope-efficiency and the grating-strength decrease with the increase of the chirp-rate.

Clearly, fibre edge-filters with arbitrary characteristics can be fabricated based on TCG structures utilising all these controllable parameters. Experimentally slope-efficiency from 0.5 dB/nm to 10 dB/nm and filtering range from 2 nm to 20 nm have been demonstrated.

As a simple demonstration, a TCG was used as an edge filter interrogating FBG strain sensor as shown in Fig. 2(a). The strain-encoded light transmitted by the tilted chirped grating was measured by an optical spectrum analyser and also by two photo detectors. Figures 2(b) and 2(c) plot the wavelength shift and optical power output against the applied strain from both measurements showing a good linearity of the edge-filter-like spectral response.

In summary, we have demonstrated a novel method for fabricating fibre edge filters with arbitrary spectral response based on TCG structures. The near-linear wavelength response with a wide range of slope-efficiencies and filtering-ranges has been realised for a series of filters.

1. S.M. Melle, K. Liu, and R.M. Measures, IEEE PTL, **4,** 516–518 (1992).
2. T. Erdogan and J.E. Sipe, Opt. Lett. **20,** 1838–1840 (1995).

## CWF71

### Retrieval of the refractive-index distributions of fiber gratings with complex Bragg reflection measurements

Ding-Wei Huang, C.C. Yang, *Department of Electrical Engineering and Institute of Electro-Optical Engineering, National Taiwan University, 1, Roosevelt Road, Sec. 4, Taipei, Taiwan, ROC; E-mail: ccy@cc.ee.ntu.edu.tw*

The Bragg reflection characteristics of a fiber grating, including intensity and phase, are controlled by its longitudinal refractive-index distribution, i.e., the local grating period and the depth of effective index modulation. Therefore, the retrieval of the longitudinal index distribution is crucially important for controlling the characteristics of a fiber grating. In this paper, we report our results of reconstructing the index distributions of a uniform and an apodized chirped fiber grating. The procedures include the measurements of their complex Bragg reflection spectra with a balanced Michelson interferometer and the execution of a simple retrieving algorithm. With the procedures, we can retrieve index profiles of fiber gratings with any apodization, chirping or dc structures.

Figure 1 shows the experimental setup for measuring the amplitude and phase of the Bragg reflection coefficient. The system was a balanced Michelson interferometer with a test arm connected to the fiber grating to be characterized and a free-space reference arm in which signal was retro-reflected by a gold-coated mirror. A tunable laser diode with a wavelength resolution of 0.001 nm was used as the light source. We measured the fiber Bragg reflection, interference, and reference intensities, respectively, by appropriately blocking light with the two attenuators. By measuring the spectra of these three intensities, the phase part of the complex reflection coefficient could be retrieved with a suitable curve fitting. After we had the complex reflection coefficient $r(z, \nu)$, we could reconstruct the complex coupling coefficient $\tilde{\kappa}(z)$. After we had $\tilde{\kappa}(z)$, we could first obtain the envelop of index profile $\delta n(z)$ through

$$\delta n(z) = |\tilde{\kappa}(z)| \cdot \frac{\lambda}{\pi}. \qquad (1)$$

Note that the dc component of index change and grating chirp are mixed in the phase of the complex coupling coefficient. Under some mild conditions, the first-order derivative of the phase of the complex coupling coefficient becomes a linear combination of the dc component, $b\delta n(z)$, of index change and grating chirp, $\alpha$, as

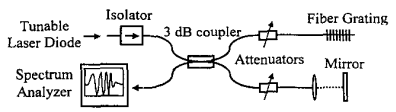


**CWF71 Fig. 1.** Schematic of the balanced Michelson interferometer used to measure the amplitude and phase of the Bragg reflection coefficient of a fiber grating.

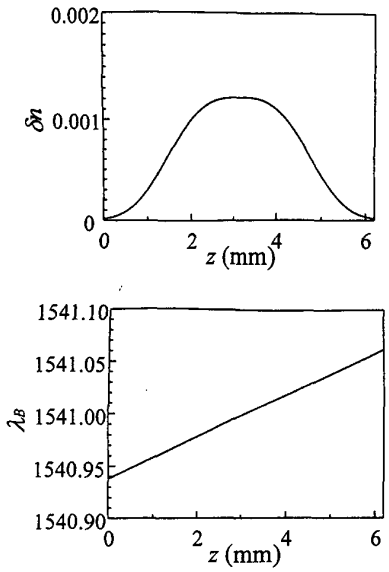


CWF71 Fig. 2. Reconstructed profiles of the index change envelop $\delta n$ (part a) and Bragg wavelength (part b) $\lambda_B$ of an apodized chirped fiber grating.

$$\frac{d\,\arg(\tilde{\kappa}(z))}{dz} = -b \cdot \frac{2\pi}{\lambda}\,\delta n(z) + \frac{2\pi}{\Lambda_0}\,\alpha \cdot z. \tag{2}$$

Here, $\Lambda_0$ is the central grating period. Then, we can use linear programming method to fit Eq. (2) for separating these two quantities.

For the apodized chirped fiber grating, the reconstructed coupling coefficient as a function of position implies a nearly-exp($-|z|^3$)-apodized profile of index change. Figure 2 shows the reconstructed profiles of the envelop of index change $\delta n$ (part a) and the local Bragg wavelength $\lambda_B$ (part b) along this fiber grating. The apodization and chirp can be clearly seen in the figures. For the uniform grating, because most signal power is Bragg reflected from a portion of grating near the input end, only the index distribution of this portion could be reconstructed. For retrieving that of the whole grating range, the complex Bragg reflection spectra at both grating ends must be measured. For both fiber gratings, the results agree very well with the fabrication conditions.

## CWF72

### Generation of side-emitting and -detecting fibers with patterned scattering zones by pulse laser treatment

R. Grunwald, H.-J. Pätzold,* H. Hart,* *Max-Born-Institute for Nonlinear Optics and Short-Pulse Spectroscopy, Rudower Chaussee 6, D-12474 Berlin, Germany; E-mail: grunwald@mbi-berlin.de*

Side-emitting and -detecting fibers are of particular interest for two classes of applications: (a) flexible light sensors with defined acceptance characteristics (spectroscopy, fill checking, safety, near field optics), (b) generation of defined light distributions and illumination of inaccessible areas or scattering environments (diffusing tips for medicine,[1] flexible sources for arts and architecture,[2] flat displays, solar light diffusors in bio-reactors). Well-known devices to transform the angular spectrum are light-induced Bragg gratings.[3] The efficiency of such high spatial frequency index gratings strongly depends on the wavelength, and the fabrication is costly.

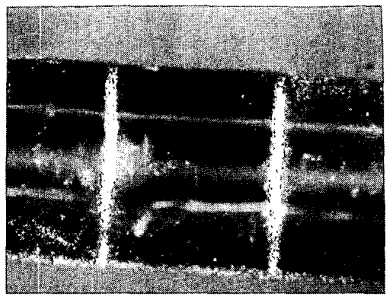

CWF72 Fig. 1. Side view of a glass fiber with periodically arranged scattering channels structured with SHG of Nd:YAG laser (5 ns, 532 nm, 2 mJ, fiber illuminated by an end-coupled He-Ne-laser, diameter of the fiber 950 μm).

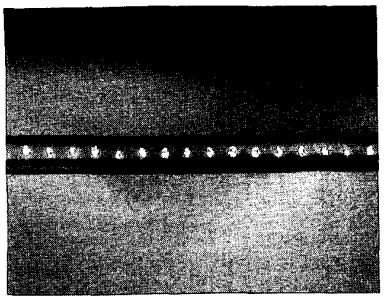

CWF72 Fig. 2. Top view of a silica fiber with periodically arranged scattering channels structured with a KrF laser (3.8 ns, 248 nm, 1 mJ, $<10^2$ pulses per channel, fiber illuminated by an end-coupled He-Ne-laser, diameter of the fiber 1500 μm).

CWF72 Fig. 3. Continuously emitting PMMA fiber structured with a KrF laser (3.8 ns, 248 nm, 1 mJ, 3 μm steps in axial direction, fiber illuminated by an end-coupled He-Ne-laser, diameter of the fiber 1500 μm).

As an alternative and simple approach, we investigated the possibility to generate periodically as well as quasi-homogeneously arranged scattering zones along fibers of different materials (glass, quartz, polymers, diameters 200 . . . 1500 μm) by laser treatment. Fibers have been irradiated with the focused beams of a KrF laser (248 nm, 3.8 ns) and the SHG of a Nd:YAG laser (532 nm, 5 ns). The positions of the foci have been controlled by moving the fiber with a 3-axis step motor system and rotating the fiber. A He-Ne-laser was coupled into the core and side-on monitored by a camera system with zoom microscope objective. The spatial distribution of the scattering has been investigated by a radiometric fiber array sensor (EMITOR, GMS Ltd., Berlin). The method also allows to generate point- or channel-like and ring-shaped single scattering regions, scattering gratings with very large periods, chirped gratings and extended light diffusing zones. Depending on wavelength and material, different modes of laser processing have been found to work successfully. With the SHG of the Nd:YAG laser, channel-like scattering zones could be formed within the core of a thick glass fiber (core diameter 950 μm, Fig. 1). Smaller core diameters lead to reduced mechanical strength due to high internal stress and are not convenient for practical purposes. Single central dots in the core with nearly radially symmetric scattering characteristics could only be achieved in silica fibers by KrF-laser processing. To improve the beam shape, unstable resonators with super-Gaussian mirrors have been implemented. The transversal emission of a He-Ne-laser beam by a periodical arrangement of scattering channels in a thick silica fiber (1.5 mm diameter) is shown in Fig. 2. Polymer fibers were strongly damaged by the SHG of Nd:YAG laser so that no defined scattering structures could be fabricated by this way. However, KrF-laser treatment yielded good results and even a homogeneous, unstructured emitting line along the fiber axis was obtained (PMMA, 1.5 mm diameter, Fig. 3). The surface damage led to much lower internal stress than in glass or silica. The specific mechanisms of laser induced optical damage (LOD) in dependence on material and laser parameters are complex and have to be the subject of future investigations. Processing with ultra-short pulses (recently demonstrated by other authors with the production of waveguides in bulk glasses by focusing 120-fs pulses from a Ti:sapphire laser[4]) seems to open more efficient channels for the multiphoton excitation and could lead to further improvements.

*Society for the Promotion of Applied Optics, Optoelectronics, Quantum Electronics and Spectroscopy (GOS), Rudower Chaussee 5, D-12489 Berlin, Germany*

1. R.L. Kozodoy, S.L. Lundahl, D. Bell, J.A. Harrington, Appl. Opt. **33**(28), 6674–6682 (1994).
2. M. Sikkens, J.P.M. Ansems, Int. Lighting Rev. **44**(3), 84–91 (1993).
3. K.O. Hill, Y. Fujii, D.C. Johnson, B.S. Kawasaki, Appl. Phys. Lett. **32**(10), 647–649 (1978).
4. Laser Focus World **34**(2), 9 (1998).